Journal of Power Sources 238 (2013) 356–365

Contents lists available at SciVerse ScienceDirect

Journal of Power Sources

journal homepage: www.elsevier.com/locate/jpowsour

$Li_4Ti_5O_{12}$ electrodes operated under hurdle conditions and SiO_2 incorporation effect

Simin Jiang, Bote Zhao, Yubo Chen, Rui Cai, Zongping Shao*

State Key Laboratory of Materials-Oriented Chemical Engineering, College of Chemistry and Chemical Engineering, Nanjing University of Technology, No. 5 Xin Mofan Road, Nanjing 210009, PR China

HIGHLIGHTS

- Si is incorporated with $Li_4Ti_5O_{12}$ in the forms of Si-doping and SiO_2-coating.
- $Li_4Ti_5O_{12}$ and SiO_2-incorporated $Li_4Ti_5O_{12}$ are tested under different conditions.
- Mechanism for "decrease–increase–decrease" cycling behavior is explained.
- SiO_2 incorporation does improve the cycling stability under hurdle conditions.

ARTICLE INFO

Article history:
Received 15 January 2013
Received in revised form
26 February 2013
Accepted 2 March 2013
Available online 14 March 2013

Keywords:
Lithium-ion battery
Lithium titanate
Anode
Hurdle condition
Elevated temperature
Silicon oxide

ABSTRACT

Lithium titanate ($Li_4Ti_5O_{12}$) and SiO_2-incorporated $Li_4Ti_5O_{12}$ are synthesized, using a facile cellulose-assisted combustion technique, as anodes for lithium-ion batteries tested under different conditions, i.e., discharge to an end potential of 1.0 V/0.01 V at room/elevated temperature (55 °C). The particles are characterized using X-ray diffraction (XRD), field-emission scanning electron microscopy (FE-SEM), nitrogen adsorption–desorption isotherms, X-ray spectrometry (EDX) and transmission electron microscopy (TEM). The results show that silicon element is successfully incorporated with $Li_4Ti_5O_{12}$ homogeneously in the forms of Si-doping and SiO_2 separate phase. When discharged in the potential range of 0.01–3.0 V, initial discharge capacities of 260 mA h g^{-1} and 298 mA h g^{-1} are obtained for the $Li_4Ti_5O_{12}$ and SiO_2-incorporated $Li_4Ti_5O_{12}$ electrodes, respectively. Both electrodes show stable cycling performance for 400 cycles (approximately 1.5 months) at room temperature between 0.01 and 3.0 V at a current density of 175 mA g^{-1}. In addition, the stability of the electrodes under hurdle conditions (0.01–3.0 V at 55 °C) are explored and discussed, and a proposed mechanism for the "decrease–increase–decrease" cycling behavior is confirmed using electrochemical impedance spectroscopy (EIS) and TEM observations. The incorporation of SiO_2 was found to improve the cycling stability under hurdle conditions.

1. Introduction

Spinel $Li_4Ti_5O_{12}$ is one of the most promising anode materials of lithium-ion batteries for applications as power sources for electric vehicles and electrochemical energy storage devices that smooth out the intermittency of wind energy and solar cells to the electric grid. The advantageous features of $Li_4Ti_5O_{12}$ over conventional carbon/graphite-based anodes include its near-zero volume change during charge and discharge cycling, its very flat voltage plateau at approximately 1.55 V higher than the reduction potential of most organic electrolytes to avoid the formation of a solid–electrolyte interface (SEI), and its high thermal stability. As a result, $Li_4Ti_5O_{12}$ electrodes usually exhibit good cycling stability and safety when operated at room temperature and discharged to an end potential of 1.0 V [1,2].

The insertion of lithium into a $Li_4Ti_5O_{12}$ spinel follows a two-phase mechanism. During the discharge process, the incoming lithium ions insert into 16c octahedral sites, and the lithium ions at 8a sites simultaneously transfer to the 16c sites. The insertion process can be expressed by the following equation:

$$Li_4Ti_5O_{12} + 3e^- + 3Li^+ = Li_7Ti_5O_{12}$$

According to this equation, a theoretical capacity of 175 mA h g^{-1} is expected based on the mass of $Li_4Ti_5O_{12}$, which is actually not very attractive. From a structural point of view, however, $Li_7Ti_5O_{12}$ could

* Corresponding author. Tel.: +86 25 8317 2256; fax: +86 25 8317 2242.
E-mail address: shaozp@njut.edu.cn (Z. Shao).

0378-7753/$ – see front matter © 2013 Elsevier B.V. All rights reserved.
http://dx.doi.org/10.1016/j.jpowsour.2013.03.017

accommodate more lithium ions because empty 8a sites are still available, although these sites are energetically less favorable than the 16c sites. Recently, a considerable increase in the total reversible capacity of $Li_4Ti_5O_{12}$ at discharge voltages less than 0.5 V has been demonstrated experimentally [3]. Zhong et al. further demonstrated that $Li_4Ti_5O_{12}$ can be intercalated to a final state of $Li_{8.5}Ti_5O_{12}$ [4] and predicted an intercalation potential of 0.05 V (vs. Li/Li^+) for the $Li_7Ti_5O_{12}/Li_{8.5}Ti_5O_{12}$ redox couple. Interestingly, the insertion of lithium into $Li_7Ti_5O_{12}$ with the formation of $Li_{8.5}Ti_5O_{12}$ also induces a small strain (approximately 0.4%). In addition, the theoretical capacity of $Li_4Ti_5O_{12}$ increases to 293 mA h g^{-1} when discharged to 0.01 V, and this capacity is limited by the number of tetravalent titanium ions [5]. Another advantage by operating $Li_4Ti_5O_{12}$ at a lower potential is the increase in cell voltage, which results in greater overall energy density.

The discharge of a $Li_4Ti_5O_{12}$ cell to a potential lower than 1.0 V, however, re-introduces the possibility of SEI film formation because most organic electrolytes have high reduction reactivity on the anode within the potential range of 1.0–0.5 V. Such an SEI film usually has the characteristics of an electrolyte, i.e., SEI films conduct lithium ions but not electrons, which may significantly affect the cycling stability of $Li_4Ti_5O_{12}$. Although some researchers have demonstrated that pristine or doped $Li_4Ti_5O_{12}$ exhibits good cycling stability when the discharge voltage is extended to 0.01 V [6,7], they usually performed their studies at room temperature. For practical applications, the batteries may face hurdle operating conditions, such as elevated temperature, which will accelerate the reaction between the electrode and the liquid electrolyte. Until now, the cycling stability of $Li_4Ti_5O_{12}$ at elevated temperature has rarely been reported, particularly under conditions of deep discharge to near-zero voltage.

Surface coating and doping could introduce several beneficial effects for electrode materials in lithium-ion batteries, such as improving the surface lithium-ion charge transfer (coating) or the bulk lithium diffusion rate (doping), increasing the electrical conductivity, and effectively avoiding or reducing direct contact between the electrode and electrolyte (coating), thus reducing the rate of catalytic decomposition of the electrolyte. Ahn et al. applied a nanometer-thick Al_2O_3 coating onto $Li_4Ti_5O_{12}$ using atomic layer deposition and found that it successfully improved the capacity retention during cycling of $Li_4Ti_5O_{12}$ at room temperature between 0.01 and 3.0 V [3]. However, the stable capacity was only 140 mA h g^{-1}, which is less than the theoretical capacity (175 mA h g^{-1}) of $Li_4Ti_5O_{12}$ for the discharge to an end voltage of 1.0 V. Lin et al. applied an amorphous silicon film as a coating material for $Li_4Ti_5O_{12}$ to operate at elevated temperatures [8]. However, the discharge capacity of the α-Si film/$Li_4Ti_5O_{12}$ decreased more dramatically than that of pristine $Li_4Ti_5O_{12}$ in the potential range of 0.0–3.0 V, partially due to Si layer delaminating from the $Li_4Ti_5O_{12}$ surface with increasing discharge rate. Such delamination is related to the large volumetric change of the Si layer during the lithium insertion/extraction process. He et al. used a carbon coating to suppress the reduction decomposition of the electrolyte on the $Li_4Ti_5O_{12}$ electrode during deep discharge to near-zero voltage [9]. However, carbon begins to incorporate lithium at near-zero voltage, which will cause a volume change of the carbon layer and detrimentally affect the long-term cycling stability of a $Li_4Ti_5O_{12}$ electrode.

Fumed SiO_2 has been widely used in the battery industry as an additive for organic electrolytes; it traps impurities, such as water, and neutralizes HF by converting them into Si–F species [10]. SiO_2 has also been used as a coating material for cathodes, including $LiFePO_4$, $Li_3V_2(PO_4)_3$/C, $LiNi_{0.5}Mn_{1.5}O_4$, $LiNi_{0.8}Co_{0.2}O_2$ and $Li_{1.03}Mn_{1.97}O_4$, to increase their cycling performance by reducing the dissolution of the electrodes into the electrolyte and neutralizing HF [10–14]. For example, a SiO_2 protective layer has been reported to efficiently decrease by more than 50% the exothermic reaction of the cathode material $LiNi_{0.8}Co_{0.2}O_2$ in the charged state with the electrolyte [13]. However, no reports related to the application of SiO_2 as a coating layer or additive for $Li_4Ti_5O_{12}$ have appeared in the literature.

In this study, we synthesized and investigated $Li_4Ti_5O_{12}$ as an anode for lithium-ion batteries to be operated under hurdle conditions, i.e., deep discharge to a potential of 0.01 V and at an elevated temperature of 55 °C, and tried to improve its performance by applying SiO_2 as an additive. The performance of the electrodes under various conditions and the effect of the incorporation of SiO_2 on the cycling stability under hurdle conditions was investigated and explained.

2. Experimental

2.1. Materials preparation

The $Li_4Ti_5O_{12}$ and $SiO_2/Li_4Ti_5O_{12}$ powders were synthesized using a cellulose-assisted combustion technique [2]. Tetrabutyl titanate [$Ti(C_4H_9O)_4$] was slowly added into de-ionized water in an ice-water bath under vigorous stirring until a white precipitate of $TiO(OH)_2$ was formed. Nitric acid was then dropped under stirring to acquire a transparent titanyl nitrate solution. Lithium nitrate ($LiNO_3$) (Li excess: 8% mol) and tetraethoxysilane (TEOS, used as a silica source, TEOS:$Li_4Ti_5O_{12}$ molar ratio = 10:100) were added, and glycine was subsequently introduced as fuel at a glycine/total metal ions molar ratio of 3:1. Natural cotton fibers were used as the cellulose sources which were pre-activated with HNO_3. The as-obtained solution was then soaked into the activated cellulose. After being dried at 80 °C, the precursors were transferred to a pre-heated electrical oven at 250 °C to trigger the auto combustion. During the auto combustion process, a strong flame appeared which lasted for 10–15 s and a subsequent gentle combustion lasted for several minutes. The primary product was then further calcined at 700 °C for 5 h in air. The $Li_4Ti_5O_{12}$ powders were synthesized using the same process without the addition of TEOS. The as-prepared $Li_4Ti_5O_{12}$ and $SiO_2/Li_4Ti_5O_{12}$ powders were named CS-LTO and CS-SiO_2/LTO.

2.2. Basic characterization

The crystal structures of the synthesized powders were characterized via X-ray diffraction (XRD) on Bruker D8 ADVANCE X-ray diffractometer equipped with a Cu Kα radiation (λ = 1.5406 Å) source; the XRD patterns were collected at room temperature. The data for Rietveld refinement collected in the 2θ range from 10° to 90° at an interval of 0.02°, and the structure refinements were performed with the GSAS software program [15,16]. Parameters such as the scale factor, the peak shape, the lattice parameters, the background and the isotropic atomic displacement parameter (U_{iso}) were refined during the refinement. The U_{iso} values at the same Wyckoff site were constrained to be equal, and the sum of occupancy parameters of all atoms at 8a or 16d sites was equal to one during the refinement of the structure parameters. Particulate morphologies were examined using field-emission scanning electron microscopy (FE-SEM, Hitachi S-4800), environmental scanning electronic microscopy (ESEM, QUANTA-200) coupled with an energy dispersive X-ray spectrometer (EDX) and transmission electron microscopy (TEM, JEOL JEM-2100). Prior to the TEM observations, the powder samples were ultrasonically dispersed in ethanol; the cells with different cycle times (stopped at 1.6 V at discharge state after cycling between 0.01 and 3.0 V at 55 °C) were disassembled in an argon-filled glove box and the electrode layer is

scraped from the current collector (Cu foil) using a lab-used knife, and then the samples were ultrasonically dispersed in dimethyl carbonate (DMC) and kept in sealed vials before TEM observations. The nitrogen adsorption–desorption curves of samples were measured at 77 K using a TriStar II 3020 instrument.

2.3. Electrode fabrication

The electrochemical performances of pristine and SiO_2-incorporated $Li_4Ti_5O_{12}$ were tested in CR2016-type coin cells using metallic lithium films as both the counter and reference electrodes. The working electrodes were prepared using a slurry coating procedure. The slurry was prepared by mixing 85 wt.% active material with 8 wt.% conductive Super P and 7 wt.% polyvinylidene fluoride (PVDF) binder in *N*-methyl pyrrolidinone (NMP) and was uniformly deposited onto copper foil current collectors. The working electrodes were subsequently dried in a vacuum oven at 100 °C overnight to volatilize possible adsorbed water and residual solvent. The cells were assembled in a glove box filled with pure argon using microporous polypropylene film (Celgard 2400) as the separator and 1 M $LiPF_6$ solution in an ethylene carbonate–dimethyl carbonate (EC–DMC, 1:1, vol/vol) mixture as the electrolyte. All the cells were allowed to age for 12 h before being tested.

2.4. Electrochemical characterization

Electrochemical performance tests were performed using an automatic galvanostat (NEWARE BTS 5 V–10 mA) with cutoff voltages of 1.0 and 3.0 V or 0.01 and 3.0 V at different current rates at room temperature or at an elevated temperature of 55 °C. Electrochemical impedance spectroscopy (EIS) measurements of the cells were performed on a Princeton Applied Research PARSTAT 2273 advanced electrochemical system in the frequency range of 100 mHz–100 kHz, and the AC modulation was controlled at 10 mV. After being cycled between 0.01 and 3.0 V at 55 °C, the cells were removed from the thermostat container and tested at 1.6 V (discharge state) for EIS.

3. Results and discussion

3.1. Phase structure

Fig. 1 shows typical XRD patterns of the pristine $Li_4Ti_5O_{12}$ (CS-LTO) and $SiO_2/Li_4Ti_5O_{12}$ composites (CS-SiO_2/LTO) prepared by the cellulose-assisted combustion technique. For both samples, the main diffraction patterns can be well indexed based on a cubic spinel structure with a space group of $Fd\bar{3}m$. No obvious peaks that correspond to a SiO_2 crystalline phase were observed in the XRD patterns of CS-SiO_2/LTO, which suggests that the SiO_2 in the $SiO_2/Li_4Ti_5O_{12}$ composite was likely in an amorphous phase or was successfully incorporated into the $Li_4Ti_5O_{12}$ lattice.

To demonstrate whether Si was potentially incorporated into the lattice structure of $Li_4Ti_5O_{12}$, the XRD patterns of both CS-LTO and CS-SiO_2/LTO were analyzed via Rietveld refinement. As shown in Fig. 2, in addition to the main $Li_4Ti_5O_{12}$ spinel phase (ICSD #160655), additional weak peaks that correspond to rutile TiO_2 (ICSD #53601) for CS-LTO and rutile TiO_2 and Li_2TiO_3 for CS-SiO_2/LTO were observed in their XRD patterns. The appearance of rutile TiO_2 in CS-LTO can be explained by the partial loss of Li through evaporation during the synthesis. Given their low contents, only the unit-cell parameters of TiO_2 and Li_2TiO_3 were refined, and the structural parameters for Li_2TiO_3 were adopted from Kataoka et al. [17]. It was unclear whether Si was doped into the 8a tetragonal or 16d octahedral sites; therefore, the original CS-LTO structural parameters were used for the Rietveld refinement of the CS-SiO_2/LTO

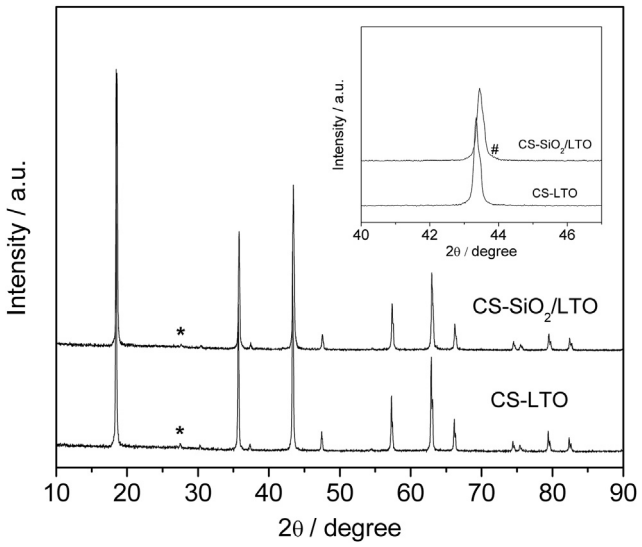

Fig. 1. XRD patterns of CS-LTO and CS-SiO_2/LTO; the peaks assigned to TiO_2 and Li_2TiO_3 are marked with (*) and (#), respectively.

XRD patterns. Although reliable results were obtained for both samples, the U_{iso} values for Li/Ti at 8a/16d sites, especially for the Li^+ doped at the 8a site, observed for the $Li_4Ti_5O_{12}$ phase in CS-SiO_2/LTO were significantly smaller than those observed for the $Li_4Ti_5O_{12}$ in CS-LTO. In addition, the unit-cell parameter of the $Li_4Ti_5O_{12}$ phase in CS-SiO_2/LTO ($a \approx 8.362$ Å) was also slightly smaller than that in CS-LTO ($a \approx 8.364$ Å). Given the greater scattering factor of Si compared to that of Li and the small ionic radii of Si^{4+} ($r(^{IV}Si^{4+}) = 0.26$ Å, $r(^{VI}Si^{4+}) = 0.40$ Å) [18], Si^{4+} was likely doped into the 8a site or into both the 8a and 16d sites. We then attempted to refine Si into the 8a and/or the 16d site of the $Li_4Ti_5O_{12}$ phase in CS-SiO_2/LTO. Negative occupancy parameters were obtained for Si at 16d octahedral site if the Si was attempted to replace Li^+/Ti^{4+} at 16d octahedral site, thus Si should be solely doped into the 8a tetragonal site. This result agreed well with the fact that silicon preferred 4-fold coordination rather than 6-fold coordination with oxygen under normal conditions [19]. To avoid the potential correlations between U_{iso} values and occupancy parameters, the U_{iso} values of Li^+ and Si^{4+} at the 8a tetragonal site were set equal with that at the 16d octahedral site and were refined together. The final refined parameters are shown in Table 1. Based on the refined

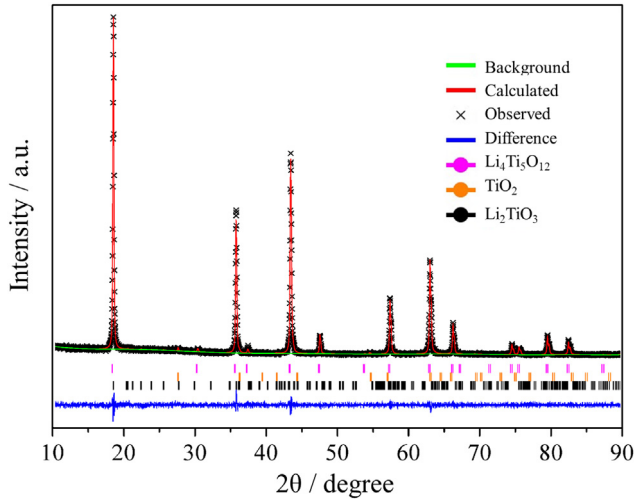

Fig. 2. Rietveld plots from XRD data for CS-SiO_2/LTO sample at room temperature.

Table 1
Crystallographic parameters and reliability factors at room temperature for CS-LTO and CS-SiO_2/LTO from XRD data.

Sample	CS-LTO	CS-SiO_2/LTO
Crystallographic parameters		
Space group	*F d* $\bar{3}$ *m*	*F d* $\bar{3}$ *m*
a (Å)	8.36442(4)	8.36276(0)
V (Å^3)	585.204(3)	584.855(9)
Li1		
Wyckoff site	8a (1/8, 1/8, 1/8)	8a (1/8, 1/8, 1/8)
Occ.	1	0.981(8)
U_{iso} (Å^2)	0.0330(9)	0.0266(2)
Si1		
Wyckoff site	8a (1/8, 1/8, 1/8)	8a (1/8, 1/8, 1/8)
Occ.	/	0.018(2)
U_{iso} (Å^2)	/	0.0266(2)
Li2		
Wyckoff site	16d (1/2, 1/2, 1/2)	16d (1/2, 1/2, 1/2)
Occ.	0.1667	0.1667
U_{iso} (Å^2)	0.0323(7)	0.0266(2)
Ti1		
Wyckoff site	16d (1/2, 1/2, 1/2)	16d (1/2, 1/2, 1/2)
Occ.	0.8333	0.8333
U_{iso} (Å^2)	0.0323(7)	0.0266(2)
O1		
Wyckoff site	32e (*z*, *z*, *z*)	32e (*z*, *z*, *z*)
z	0.2623(9)	0.2616(1)
Occ.	1	1
U_{iso} (Å^2)	0.0354(0)	0.0319(9)
Weight percentage (%)		
$Li_4Ti_5O_{12}$	98.9(2)	98.1(2)
TiO_2	1.0(8)	0.69(1)
Li_2TiO_2	/	1.18(9)
Reliability factors		
χ^2	1.21	1.14
R_p (%)	6.45	6.41
R_{wp} (%)	7.44	7.50
R_{Bragg} (%)	7.80	9.52

results, a Si/Ti mole ratio of 0.0107(2):1 was obtained, which was lower than the nominal Si/Ti molar ratio of 0.02:1. This result suggests partial silicon elements (~46.5%) were not incorporated into the spinel lattice; however, the residual silicon was too low to be detected by XRD or was present as an amorphous phase.

3.2. Particulate morphology

Particulate morphologies of the pristine $Li_4Ti_5O_{12}$ and the SiO_2/$Li_4Ti_5O_{12}$ composite prepared via the combustion synthesis were examined using FE-SEM, and typical images are shown in Fig. 3. The CS-LTO sample was composed of nanoparticles that were severely aggregated to form large porous grains, and macropores were

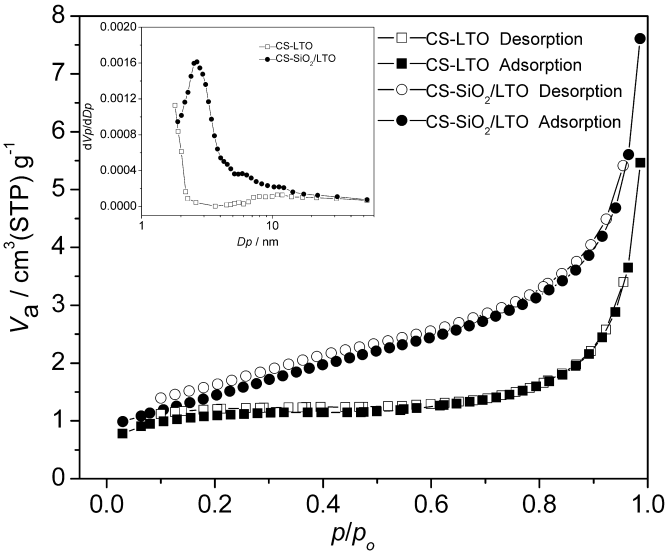

Fig. 4. The nitrogen adsorption–desorption curves of CS-LTO and CS-SiO_2/LTO and the BJH pore size distribution curves of the samples (inset).

observed. With respect to the CS-SiO_2/LTO sample, similar particulate morphology was also observed, and some macropores with diameters of several hundred nanometers were also clearly observed. The nitrogen adsorption–desorption isotherms of both samples were subsequently measured to obtain further information about their microstructures. The CS-LTO and CS-SiO_2/LTO exhibited BET specific surface areas of 3.57 and 5.66 $m^2\ g^{-1}$, respectively. The greater surface area of CS-SiO_2/LTO compared to that of CS-LTO suggests that SiO_2 suppressed the sintering of $Li_4Ti_5O_{12}$. Fig. 4 shows the adsorption/desorption isotherm curves of both samples, and the pore size distribution profiles are presented as insets in the figure. The CS-LTO contained almost no micro- or mesopores. With respect to CS-SiO_2/LTO, although mesopores with a peak pore diameter of approximately 3 nm were present according to the pore size distribution curve, the pore volume was actually very small, with a value of 0.012 $cm^3\ g^{-1}$. Thus, the micro- and mesopores in both CS-LTO and CS-SiO_2/LTO samples can be treated as negligible.

Based on the previously discussed XRD analysis, silicon was only partially (~53.5%) doped into the $Li_4Ti_5O_{12}$ lattice; thus, some SiO_2 was also present as a separate phase. The CS-SiO_2/LTO sample was therefore further analyzed using EDX mapping; the results are shown in Fig. 5 and indicate that all of the Si, O and Ti were distributed homogeneously within the particles. This result suggests that the residual SiO_2 likely formed a coating layer over the $Li_4Ti_5O_{12}$ particles instead of forming separated particles.

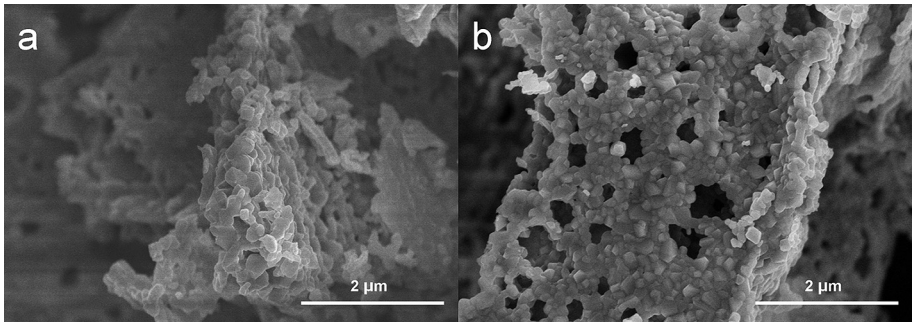

Fig. 3. FE-SEM images of (a) CS-LTO and (b) CS-SiO_2/LTO.

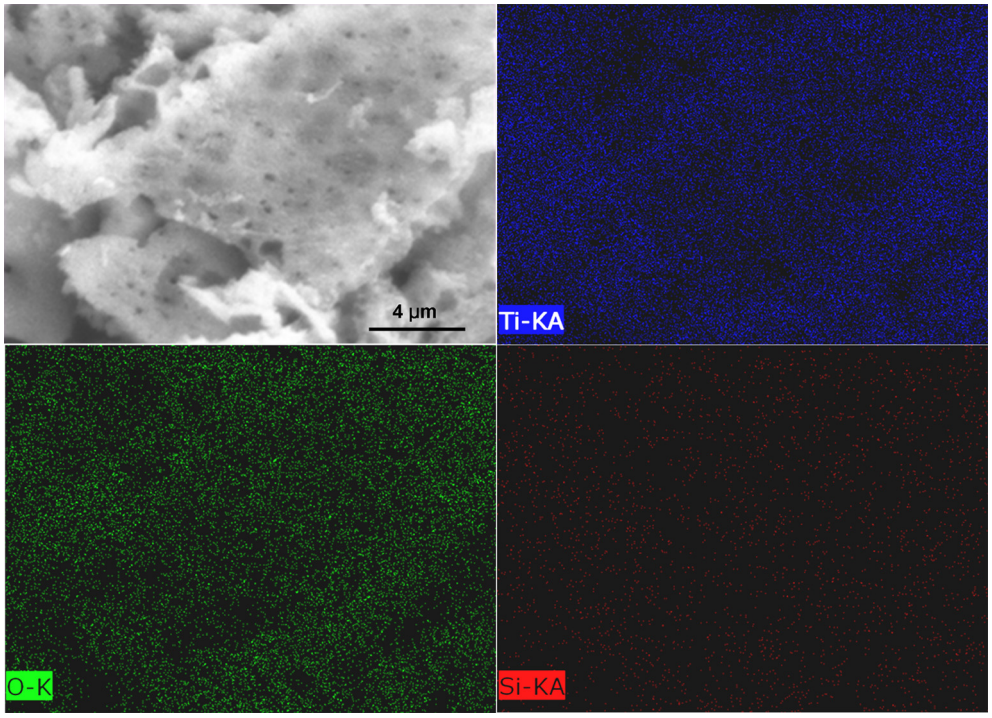

Fig. 5. SEM image of CS-SiO_2/LTO powder and the corresponding EDX mapping of Ti, O and Si.

The CS-SiO_2/LTO sample was subsequently subjected to analyses via TEM and HR-TEM to obtain direct information related to its presence of SiO_2 in the sample. As shown in Fig. 6, the primary particles exhibited an irregular grain shape and had a particle size of approximately 100 nm. HR-TEM demonstrated that the bulk phase had a fringe distance of 0.48 nm, which is in good agreement with the d-spacing of the (111) lattice plane for the $Li_4Ti_5O_{12}$ spinel; in addition, the corresponding selected-area electron diffraction (SAED) pattern of the bulk phase could be well indexed based on the (111), (311) and (333) lattice planes of the spinel $Li_4Ti_5O_{12}$ phase, which suggests that the bulk phase of the particles was composed of crystallized $Li_4Ti_5O_{12}$ spinel phase. Almost no SiO_2 coating was observed. By assuming a spherical particulate morphology, a mean particle diameter of 100 nm and a homogeneous coating, combined with the weight percentage of 1.3 wt.% SiO_2 in the sample and a 46.6% percentage of SiO_2 as a separate phase, we calculated that the SiO_2 layer thickness was only approximately 0.3 nm. Such an ultrathin layer was difficult to

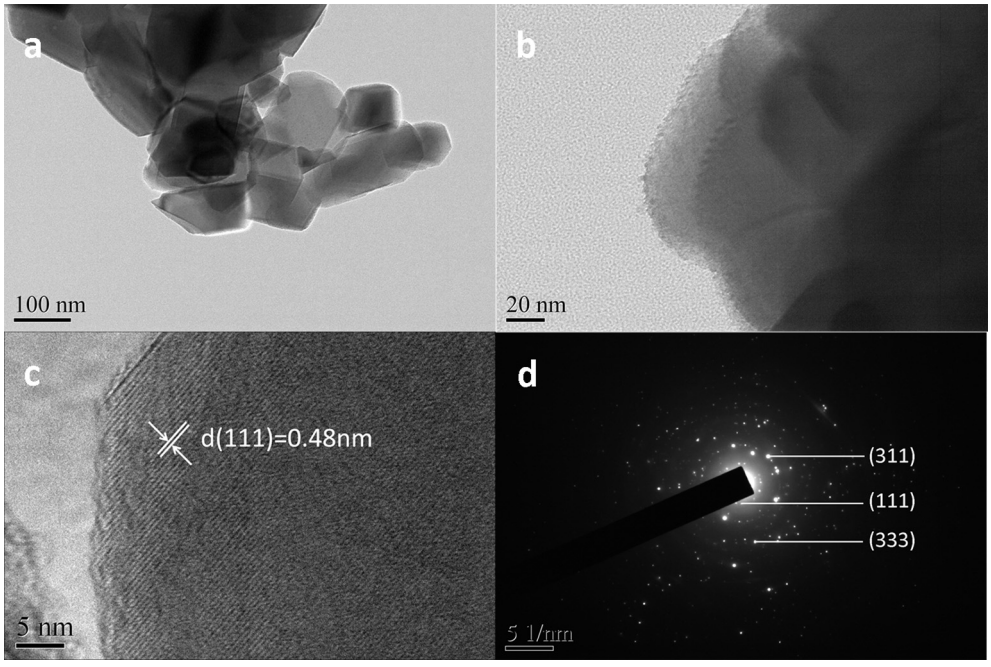

Fig. 6. (a, b) TEM and (c) HR-TEM images and (d) the SAED pattern of CS-SiO_2/LTO sample.

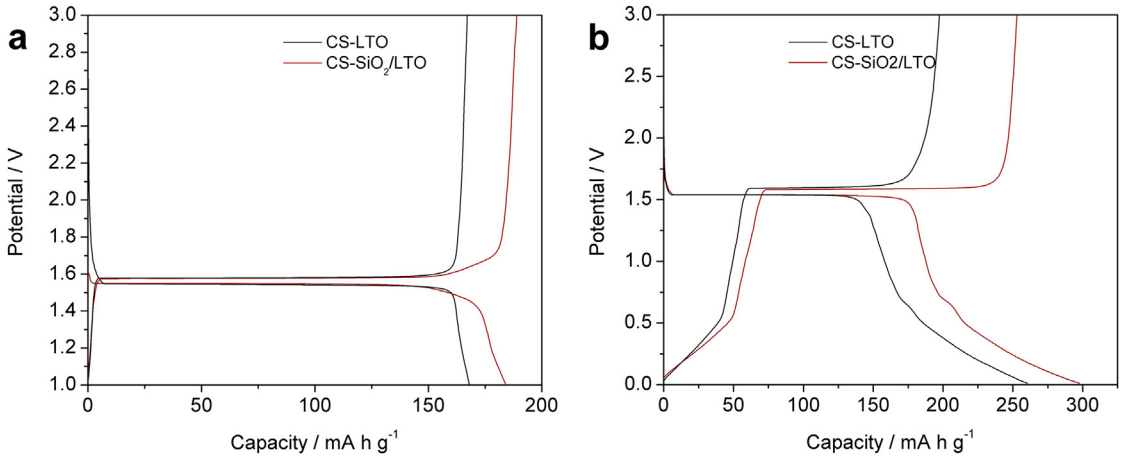

Fig. 7. The first discharge/charge profiles of CS-LTO and CS-SiO_2/LTO using a current density of 175 mA g^{-1} in the potential ranges of (a) 1.0–3.0 V and (b) 0.01–3.0 V.

detect with our TEM apparatus. To observe the morphology of the SiO_2, we synthesized SiO_2-incorporated $Li_4Ti_5O_{12}$ using the same combustion synthesis method but increased the amount of the silicon raw material 10-fold. A clear 2–3 nm homogeneous amorphous SiO_2 layer coating over the well-crystallized silicon-doped $Li_4Ti_5O_{12}$ particles was then observed (TEM images not shown here). Thus, the separate SiO_2 phase likely formed a very thin coating over the $Li_4Ti_5O_{12}$ phase.

3.3. Capacity and cycling performance under various conditions

3.3.1. Initial capacities and rate performance

Fig. 7 shows the initial discharge profiles of CS-LTO and CS-SiO_2/LTO within a potential range of 1.0–3.0 V or 0.01–3.0 V. A clear discharge plateau at approximately 1.5 V was observed for both samples, which is typical for a two-phase lithium-insertion process. At a 1 C rate, a capacity of approximately 184 mA h g^{-1} was observed for CS-SiO_2/LTO, whereas a capacity of 168 mA h g^{-1} was observed for CS-LTO when the cells were discharged within a potential range of 1.0–3.0 V. As shown in Fig. 8, a progressive decrease in capacity was observed with increased discharge rate; however, a high capacity of 142 mA h g^{-1} was still maintained even at a discharge rate of 1750 mA g^{-1} (10 C) for the CS-SiO_2/LTO electrode during discharge between 1.0 and 3.0 V, which was slightly greater than that obtained with CS-LTO (129 mA h g^{-1}). At each corresponding discharge rate, the CS-SiO_2/LTO electrodes always showed slightly greater capacity than the CS-LTO electrodes. For example, the capacities for CS-LTO were 159, 146, 129, 104 and 73 mA h g^{-1} at discharge rate of 350, 875, 1750, 3500 and 7000 mA g^{-1}, respectively, whereas the corresponding values for the CS-SiO_2/LTO were 165, 157, 142, 125 and 87 mA h g^{-1}, respectively. The greater capacity of CS-SiO_2/LTO electrodes compared to those of CS-LTO electrodes can be attributed to the greater specific surface area of the former, which ensured a shorter lithium diffusion distance in the particles as well a greater surface area for the interfacial charge transfer. On the other hand, it implies that the thin-film SiO_2 coating and the slight Si doping negligibly affected the lithium intercalation into the $Li_4Ti_5O_{12}$ lattice.

When the cells were discharged in a potential range of 0.01–3.0 V, much higher capacity was observed at various rates than when the cells were discharged to an end potential of 1.0 V. For example, for the CS-LTO electrode, an initial discharge capacity of 260 mA h g^{-1} was obtained for the discharging between 0.01 and 3.0 V; in comparison, discharge to an end potential of 1.0 V resulted in a capacity of 168 mA h g^{-1}. For the CS-SiO_2/LTO electrode, a slightly higher discharge capacity of 298 mA h g^{-1} was achieved. From Fig. 7, a significant increase in the capacity at potential lower than 0.5 V was observed for both electrodes when they were discharged between 0.01 and 3.0 V. When the discharge rates were increased, the capacities of both electrodes decreased; however, CS-SiO_2/LTO still exhibited a capacity greater than that of CS-LTO at the same discharge rates. Even at a high discharge rate of 7000 mA g^{-1},

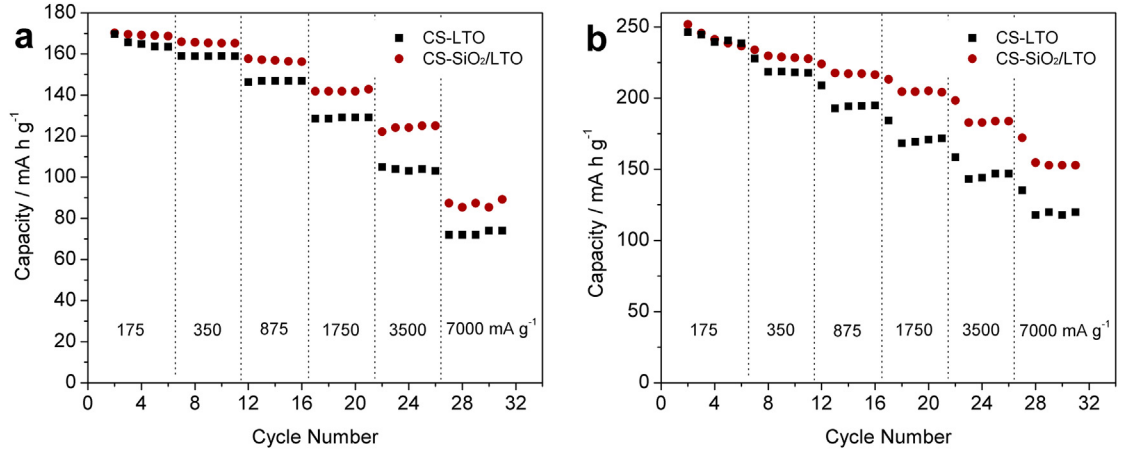

Fig. 8. Cycling performance of the CS-LTO and CS-SiO_2/LTO at different current densities between (a) 1.0 and 3.0 V and (b) 0.01 and 3.0 V.

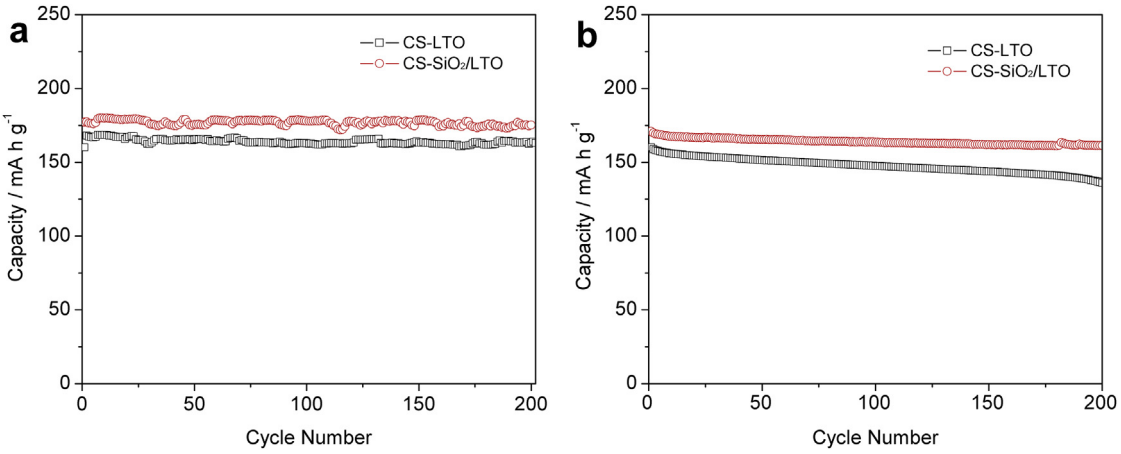

Fig. 9. Cycling performance of the CS-LTO and CS-SiO_2/LTO at (a) room temperature and (b) 55 °C between 1.0 and 3.0 V (discharge/charge current density: 175 mA g^{-1}).

CS-SiO_2/LTO exhibited a capacity of 155 mA h g^{-1}, which is approximately two times greater than that achieved when CS-SiO_2/LTO was discharged to 1.0 V (87 mA h g^{-1}). This result suggests that discharge to lower potential effectively increased the capacity.

3.3.2. Cycling stability within the potential range of 1.0–3.0 V

The cycling stability for the samples with and without the SiO_2 modification between the potential range of 1.0 and 3.0 V at room temperature and 55 °C are shown in Fig. 9. Both samples showed fairly good cycling stability within a test period of 200 cycles. At room temperature, capacities of approximately 165 and 175 mA h g^{-1} were maintained for CS-LTO and CS-SiO_2/LTO, respectively, at a discharge rate of 175 mA g^{-1}. Such a high cycling stability was clearly related to the high-end discharge potential (1.0 V), above the decomposition of liquid electrolyte to form SEI over the electrode particles on the one hand, and the zero strain nature of the $Li_4Ti_5O_{12}$ during the lithium electrochemical insertion/extraction process on the other hand. The CS-SiO_2/LTO electrode also exhibited fairly good cycling stability at 55 °C, with stable capacity of approximately 166 mA h g^{-1}. However, CS-LTO exhibited a slight decrease in capacity with increased cycling time, and the capacity was reduced from 160 mA h g^{-1} at the first cycle to 136 mA h g^{-1} at the 200th cycle. The slight decrease in capacity of pristine $Li_4Ti_5O_{12}$ when discharged in the potential range of 1.0–3.0 V at 55 °C suggests that a reaction between $Li_4Ti_5O_{12}$ and the liquid electrolyte may have occurred, whereas the slight Si doping and/or SiO_2 surface coating likely suppressed such a reaction and thus led to improved cycling stability of the CS-SiO_2/LTO electrode.

3.3.3. Cycling stability within the potential range of 0.01–3.0 V

Fig. 10a shows the cycling performance of discharge capacities of the electrodes between 0.01 and 3.0 V at room temperature and at a constant discharge rate of 175 mA g^{-1}. Before the stability test, the cells were activated for several cycles. A decrease in capacity from an initial value of 229 mA h g^{-1} at the first cycle to approximately 206 mA h g^{-1} at the 20th charge–discharge cycle was observed at the initial stage of the cycling tests for the CS-LTO electrodes; the discharge capacity then further slowly decreased to approximately 203 mA h g^{-1} after 50 charge–discharge cycles. With further cycling, a slight and steady increase in the discharge capacity with increasing cycling times was instead observed; the capacity reached a value of 223 mA h g^{-1} at 200 cycles. The capacity was still improved with cycling time even after 400 charge–discharge cycles. Afterwards, the experiment was mandatorily stopped. For the CS-SiO_2/LTO electrode, the decay in capacity during the initial 20 cycles was smaller than that observed for the CS-LTO electrode; the capacity decreased from an initial value of 228 to 215 mA h g^{-1} at the 20th cycle. In addition, a slow decrease in capacity to 212 mA h g^{-1} was also observed after 46 charge–discharge cycles. The capacity then experienced a slow but steady increase, which was almost linear with respect to the cycling time, to approximately 224 mA h g^{-1} at the 200th cycle. Similar to the performance

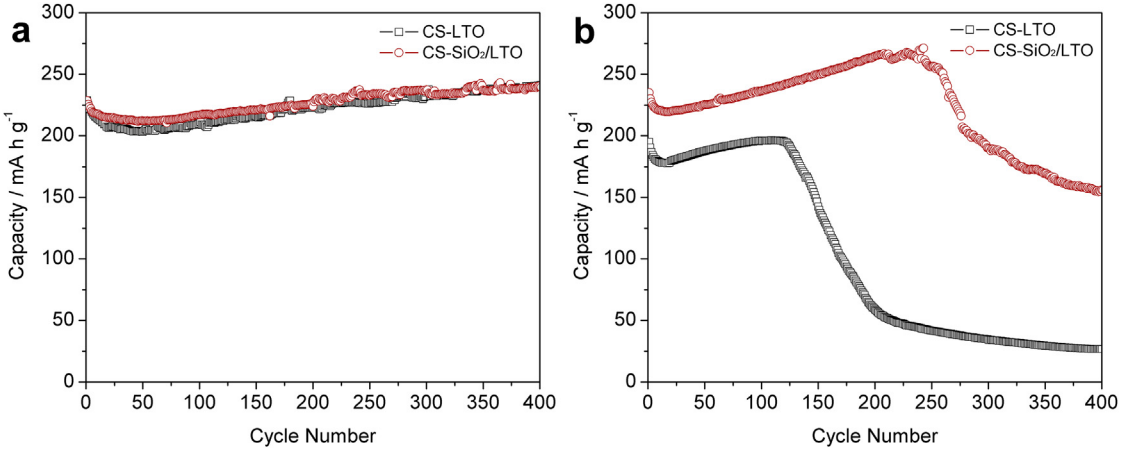

Fig. 10. Cycling performance of the CS-LTO and CS-SiO_2/LTO at (a) room temperature and (b) 55 °C between 0.01 and 3.0 V (discharge/charge current density: 175 mA g^{-1}).

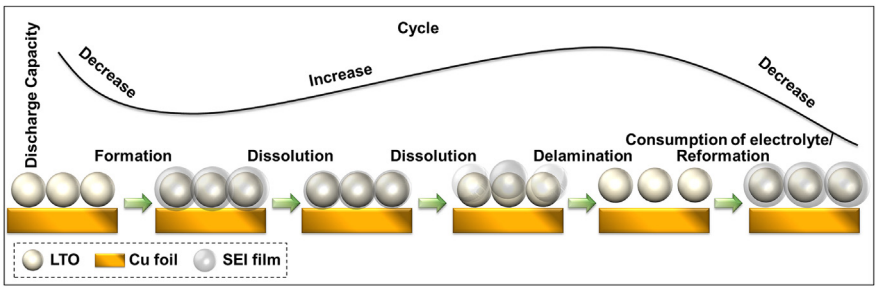

Fig. 11. The schematic illustration of mechanism for the "decrease–increase–decrease" cycling behavior of $Li_4Ti_5O_{12}$ between 0.01 and 3.0 V at 55 °C.

of CS-LTO, the slow increase in the capacity of CS-SiO_2/LTO after 400 charge–discharge cycles still did not stop.

An initial decrease in capacity for $Li_4Ti_5O_{12}$ electrode discharged to 0.01 V at room temperature was also observed by several researchers. For example, Yi et al. investigated the cycling performance of $Li_4Ti_{4.95}V_{0.05}O_{12}$ and $Li_4Ti_5O_{12}$ within a potential range of 0.0–2.5 V; they observed a relatively rapid decrease in capacity during the initial 15 cycles and a slow decrease in the subsequent 35 cycles [20]. For $Li_4Ti_5O_{12}$ both bare and coated with an ultrathin Al_2O_3 layer, Ahn et al. also observed a decrease in capacity within the initial 20 cycles [3]. Tian et al. also observed a decrease in capacity for both $Li_4Ti_5O_{12}$ and Nb-doped $Li_4Ti_5O_{12}$ between 0.0 and 2.5 V [21]. Based on CVs and EIS results, they demonstrated that such a decrease in capacity was due to the formation of an SEI film.

The cycling stability of CS-LTO and CS-SiO_2/LTO at an elevated temperature of 55 °C was also investigated; the results are shown in Fig. 10b. Prior to the elevated temperature stability test, the cells were activated for several cycles at room temperature between 0.01 and 3.0 V. We found that the initial decay in capacity with cycling time was accelerated and that the minimum capacity was reached at the 17th/16th cycle for both samples, in comparison to the 50th/46th cycle for cells cycled at room temperature. These results suggest that the kinetics of the formation of SEI films were improved at an elevated temperature. Notably, the initial capacity during the cycling for the CS-LTO sample was less than that observed at room temperature; however, the initial capacity of the CS-SiO_2/LTO was almost the same compared to that at room temperature. The thickness of the SEI layer has been reported to increase at elevated temperature in an ethylene carbonate solution: from 16 nm at 30 °C to 50 nm at 60 °C [22]. We therefore suggested that the lower initial capacity for CS-LTO at 55 °C was mainly due to the rapid increase in the thickness of the SEI layer with increased temperature. However, the SiO_2 surface coating likely suppressed such a reaction in the CS-SiO_2/LTO electrode.

Because the lithium conductivity in $Li_4Ti_5O_{12}$ should increase with an increase in the operating temperature, the lithium diffusion within the $Li_4Ti_5O_{12}$ particle interior was less likely the rate-limiting step for lithium insertion into both CS-LTO and CS-SiO_2/LTO electrodes. After the minimum capacity was reached at the 17th/16th cycle, an increase in capacity with increased cycling time was observed for both samples, and linear characteristics were also observed. However, the capacity of the CS-LTO electrode, after the electrode was cycled 115 times to reach a capacity of 196 mA h g^{-1}, sharply decreased as the cycling time increased further and decreased to only 59 mA h g^{-1} after 200 charge–discharge cycles. For the CS-SiO_2/LTO electrode, the slow increase in capacity was prolonged until it reached a maximum capacity of 271 mA h g^{-1} at 243 cycles; it then exhibited a sharp decrease in capacity to approximately 190 mA h g^{-1} at 300 cycles. These results suggest that the Si doping and/or the SiO_2 surface coating effectively increased the cycling stability of $Li_4Ti_5O_{12}$ at elevated temperatures, even though the amount of SiO_2 was very low. In comparison with their performance at room temperature, it is obvious that the degradation at high temperature was increased for both CS-LTO and CS-SiO_2/LTO electrodes.

Based on previously published results and on the cycling performance, we hypothesized a possible mechanism for the "decrease–increase–decrease" cycling behavior of $Li_4Ti_5O_{12}$ between 0.01 and 3.0 V at elevated temperature, as shown in Fig. 11. The initial decrease in capacity was due to the formation of an SEI film. After a certain number of cycles, the particles were completely covered by a thick SEI film, and the SEI film slowly dissolved. The dissolution of the SEI film during cycling has also been observed and discussed by numerous authors based on computer simulations and experiments, especially at elevated temperatures [23–25]. The SEI film was most likely partially dissolved during the cycling, which reduced the SEI thickness; as a result, the electrode capacity progressively increased. However, the decomposition of liquid electrolyte over the electrode also produced gaseous products, which finally caused the delamination of the SEI films from

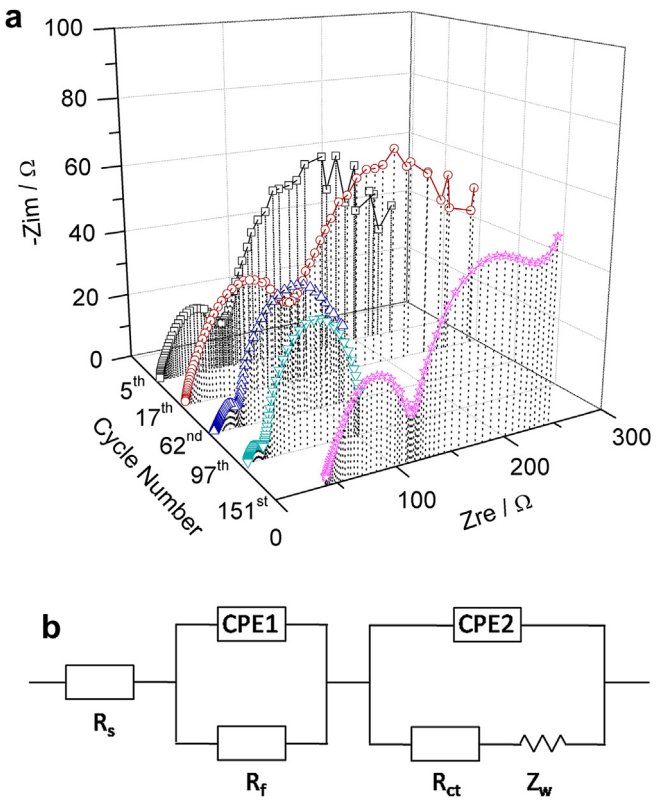

Fig. 12. (a) Impedance spectra of CS-LTO at different cycle times (tested at 1.6 V after cycling between 0.01 and 3.0 V at 55 °C); (b) equivalent circuit.

Table 2
Values of the R_s, R_f and R_{ct} obtained by simulating the date of Fig. 12a.

Cycling time	R_s/Ω	R_f/Ω	R_{ct}/Ω
5th	2.903	63.27	181.1
17th	2.623	105.5	199.7
62nd	3.426	23.84	101.3
97th	5.723	14.86	85.62
151st	39.69	80.93	95.12

the electrode surfaces. After further cycling, the heavy dissolution and/or delamination of the SEI film resulted in a large area of the electrode surface being exposed to the electrolyte, which accelerated irreversible reactions with the liquid electrolyte that resulted in a rapid decrease in capacity. The dissolution and/or delamination of the electrolyte became more pronounced at elevated temperature (55 °C). The SEI film then reformatted; however, the fading of the cell was irreversible. Fig. 10b shows that a small amount of SiO_2 incorporated into $Li_4Ti_5O_{12}$ can effectively increase the cycling stability under hurdle conditions, i.e., deep discharge to 0.01 V and elevated temperature. The SiO_2 can reduce the amount of direct contact of the $Li_4Ti_5O_{12}$ electrode with the liquid electrolyte; however, the SiO_2 and the formed SEI are apparently still permeable to the liquid electrolyte. Thus, the reformation of the SEI and the dissolution of the SEI occurred simultaneously.

To support this proposed mechanism of abnormal cycling behavior of CS-LTO electrodes within the potential range of 0.01–3.0 V at an elevated temperature (55 °C), the electrodes, after being cycled for different cycle times, were subjected to EIS measurements and TEM observations at room temperature. For the electrodes tested in the potential range of 1.0–3.0 V, the EIS results showed only a single depressed semicircle in the high-to-medium frequency range and a sloped line at low frequencies [2]. The EIS results of the electrodes cycled in a potential range of 0.01–3.0 V at 55 °C showed two partially overlapped semicircles in the high-to-medium frequency range (Fig. 12a). The appearance of an additional semicircle at high frequencies was attributed to the formation of an SEI film after the electrodes were cycled in the potential range between 0.01 and 3.0 V. The equivalent circuit shown as an inset in Fig. 12b was used to fit the impedance spectroscopy data; the results are shown in Table 2. The EIS results of the depressed semicircle at high frequencies were attributed to the polarization resistance (R_f) and to CPE1 of the SEI film, and the depressed semicircle at high-to-medium frequencies was attributed to the charge-transfer resistance (R_{ct}) and to CPE2. The sloped line at low frequencies corresponded to the Warburg impedance (Z_w), which is related to the lithium-ion diffusion within the particles.

As shown in Fig. 12a, after being cycled at 55 °C in the potential range of 0.01–3.0 V for 5 cycles, a large semi-arc was observed in the high frequency range, which was attributed to the formation of an SEI film. The TEM observations also confirmed that a thin amorphous SEI layer was formed after 5 cycles compared with the sample assembled in the cell without an electrochemical test (Fig. 13a and b). The sizes of the semi-arcs in the high (SEI) and high-to-medium (charge transfer) frequency ranges increased after 17 cycles. These results confirmed the first “decrease” assumption shown in Fig. 11. The sizes of both the high-frequency semi-arc (SEI) and the semi-arc at high-to-medium frequencies (charge transfer) were progressively diminished with increased cycling time, whereas the capacity progressively increased. The decrease in the polarization resistance of the SEI film was more significant than the charge transfer polarization resistance. SEI is well known to still conduct lithium ions but be insulating for electrons. The reduced polarization resistance for lithium diffusion in the SEI layer confirmed that the SEI was partially dissolved into the liquid electrolyte with increased cycling. As shown in Fig. 13c, the amorphous coating layer disappeared at the 97th cycle, which confirms the heavy dissolution and/or delamination of the SEI film. After the test for 151 cycles for pristine $Li_4Ti_5O_{12}$, a sharp increase in both the polarization resistance related to the SEI film and the charge transfer process were observed. Fig. 13d shows a TEM image of the $Li_4Ti_5O_{12}$ particle at the 181st cycle that supporting the reformation of SEI film.

Interestingly, the cell ohmic resistance (R_s), which is the sum of the electrolyte resistances of the contactor and the electrode, was also increased several times. This result suggests that the electrolyte was rapidly consumed by reactions between the electrolyte and the electrode. Furthermore, the gaseous products from the reaction become highly active at high temperatures, which led to a loss of the electric conduction between the electrode and the current collector and to the detachment of the conducting additive

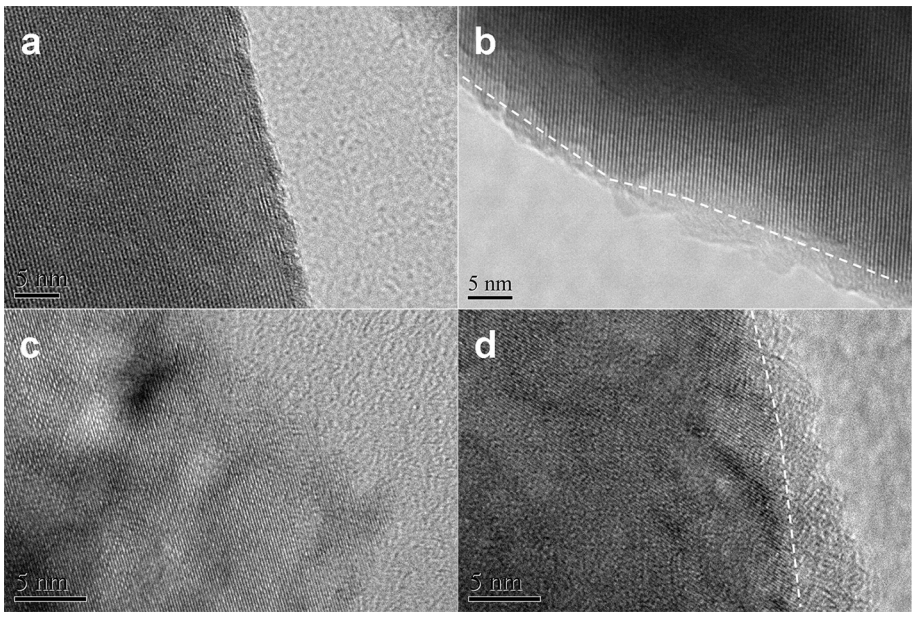

Fig. 13. TEM images of CS-LTO sample at different cycle times (stopped at 1.6 V at discharge state after cycling between 0.01 and 3.0 V at 55 °C): (a) 0; (b) 5th; (c) 97th; (d) 181st.

from the electrode particles. As a result, the effective electrode contact area was significantly reduced compared to the geometric electrode surface area; thus, the entire cell resistance, including the ohmic resistance, the SEI polarization resistance and the charge transfer resistance, was simultaneously increased.

All of the EIS and TEM results confirmed our proposed mechanism, as shown in Fig. 11. The interesting cycling performance of the CS-LTO at an elevated temperature (55 °C) between 0.01 and 3.0 V is closely related to the SEI film formation/dissolution and to the reaction between the electrode and electrolyte, but not to the material structure. We suggest that the increased cycling stability of $Li_4Ti_5O_{12}$ with SiO_2 incorporation between 0.01 and 3.0 V at 55 °C is mainly due to the SiO_2 surface coating instead of Si doping. The coated SiO_2 layer acted as a protective layer that inhibited the "decrease–increase–decrease" process caused by the reaction between the electrode and the electrolyte. On the other hand, the SiO_2 layer prevented the electrode particles against corrosion by HF by converting them into Si-F species, which resulted in a stable electrode structure [10,11]. The CS-SiO_2/LTO cell, after hundreds of cycles between 0.01 and 3.0 V at 55 °C, was disassembled in an argon-filled glove box, and the electrode was found to be relatively dry. The liquid electrolyte was then re-introduced, and the CS-SiO_2/LTO electrode was re-assembled with a new metallic lithium film and a new separator and was tested. After 1 cycle between 0.01 and 3.0 V at 55 °C, the discharge capacity increased to 235 mA h g^{-1}, and the capacity increased with increased cycling time. These results indicated that the cell was revived and that the CS-SiO_2/LTO electrode structure was stable and confirmed that the sharp decrease in capacity was caused primarily by the rapid consumption of the electrolyte. Thus, a small amount of SiO_2 incorporation can effectively increase the cycling stability of $Li_4Ti_5O_{12}$ under hurdle conditions.

4. Conclusions

In summary, $Li_4Ti_5O_{12}$ and SiO_2-incorporated $Li_4Ti_5O_{12}$ were successfully prepared via a facile cellulose-assisted combustion technique. XRD Rietveld refinement suggested that silicon was partially (~53.5%) doped into the $Li_4Ti_5O_{12}$ spinel lattice and that some SiO_2 (~46.5%) was also present as a separate phase. The results also indicated that silicon was distributed homogeneously within the particles. The SiO_2-incorporated $Li_4Ti_5O_{12}$ electrodes showed good performance under various conditions compared to that of pure $Li_4Ti_5O_{12}$ electrodes. Based on the rate performance tests, where the cells were tested in the potential range of 1.0–3.0 V, the discharge capacities for CS-LTO and CS-SiO_2/LTO were 159, 129 and 73 mA h g^{-1} and 165, 142 and 87 mA h g^{-1}, at rates of 350, 1750 and 7000 mA g^{-1}, respectively. When tested in the potential range of 0.01–3.0 V, the corresponding values for the CS-LTO and CS-SiO_2/LTO electrodes increased to 218, 170 and 120 mA h g^{-1} and to 229, 205 and 155 mA h g^{-1}, respectively. Both electrodes exhibited stable cycling performance for 200 cycles between 1.0 and 3.0 V and for 400 cycles between 0.01 and 3.0 V at room temperature (discharge/charge current density of 175 mA g^{-1}). Interestingly, under hurdle conditions (i.e., deep discharge to a potential of 0.01 V and an elevated temperature of 55 °C), both electrodes exhibited a "decrease–increase–decrease" cycling behavior, and the proposed mechanism of "SEI film formation–SEI dissolution/delamination–SEI reformation/consumption of electrolyte" was confirmed using EIS and TEM. In addition, the incorporation of SiO_2 was found to effectively increase the cycling stability of $Li_4Ti_5O_{12}$. Moreover, the high-temperature stability of $Li_4Ti_5O_{12}$ can be further improved through further research related to electrolyte additives and more stable electrolyte.

Acknowledgements

This work was partially supported by the "National Science Foundation for Distinguished Young Scholars of China" under contract No. 51025209, by "Key Projects in Nature Science Foundation of Jiangsu Province" under contract No. BK2011030, and by "National Nature Science Foundation of China" under contract No. 21103089.

References

[1] K. Zaghib, M. Dontigny, A. Guerfi, J. Trottier, J. Hamel-Paquet, V. Gariepy, K. Galoutov, P. Hovington, A. Mauger, H. Groult, C.M. Julien, J. Power Sources 216 (2012) 192–200.
[2] T. Yuan, R. Cai, K. Wang, R. Ran, S.M. Liu, Z.P. Shao, Ceram. Int. 35 (2009) 1757–1768.
[3] D.J. Ahn, X.C. Xiao, Electrochem. Commun. 131 (2011) 796–799.
[4] Z.Y. Zhong, C.Y. Ouyang, S.Q. Shi, M.S. Lei, Chem. Phys. Chem. 9 (2008) 2104–2108.
[5] H. Ge, N. Li, D.Y. Li, C.S. Dai, D.L. Wang, J. Phys. Chem. C 113 (2009) 6324–6326.
[6] H. Ge, N. Li, D.Y. Li, C.S. Dai, D.L. Wang, Electrochem. Commun. 10 (2008) 719–722.
[7] Y.R. Jhan, J.G. Duh, Electrochim. Acta 63 (2012) 9–15.
[8] Y.B. Lin, Y.M. Yang, Y. Lin, G.Y. Zhao, T. Zhou, Z.G. Huang, Int. J. Electrochem. Sci. 6 (2011) 5588–5596.
[9] Y.B. He, F. Ning, B.H. Li, Q.S. Song, W. Lv, H.D. Du, D.Y. Zhai, F.Y. Su, Q.H. Yang, F.Y. Kang, J. Power Sources 202 (2012) 253–261.
[10] Y.K. Fan, J.M. Wang, Z. Tang, W.C. He, J.Q. Zhang, Electrochim. Acta 52 (2007) 3870–3875.
[11] Y.D. Li, S.X. Zhao, C.W. Nan, B.H. Li, J. Alloys Compd 509 (2011) 957–960.
[12] L.L. Zhang, G. Liang, G. Peng, F. Zou, Y.H. Huang, M.C. Croft, A.A. Ignatov, J. Phys. Chem. C 116 (2012) 12401–12408.
[13] H. Omanda, T. Brousse, C. Marhic, D.M. Schleich, J. Electrochem. Soc. 151 (2004) A922–A929.
[14] Z.S. Zheng, Z.L. Tang, Z.T. Zhang, W.C. Shen, Y.H. Lin, Solid State Ionics 148 (2002) 317–321.
[15] A.C. Larson, R.B. Von Dreele, Los Alamos National Laboratory Report LAUR (1994), pp. 86–748.
[16] B.H.J. Toby, Appl. Cryst. 34 (2001) 210–213.
[17] K. Kataoka, Y. Takahashi, N. Kijima, H. Nagai, J. Akimoto, Y. Idemoto, K. Ohshima, Mater. Res. Bull. 44 (2009) 168–172.
[18] R.D. Shannon, Acta Cryst. A32 (1976) 751–767.
[19] J.A. Duffyand, D.E. Macphee, J. Phys. Chem. B 111 (2007) 8740–8745.
[20] T.F. Yi, J. Shu, Y.R. Zhu, X.D. Zhu, R.S. Zhu, A.N. Zhou, J. Power Sources 195 (2010) 285–288.
[21] B.B. Tian, H.F. Xiang, L. Zhang, H.H. Wang, J. Solid State Electrochem. 16 (2012) 205–211.
[22] M. Inaba, H. Tomiyasu, A. Tasaka, S.K. Jeong, Y. Iriyama, T. Abe, Z. Ogumi, Electrochemistry 71 (2003) 1132–1135.
[23] K. Tasaki, S.J. Harris, J. Phys. Chem. C 114 (2010) 8076–8083.
[24] M. Inaba, H. Tomiyasu, A. Tasaka, S.K. Jeong, Z. Ogumi, Langmuir 20 (2004) 1348–1355.
[25] A.M. Andersson, K. Edström, J.O. Thomas, J. Power Sources 81–82 (1999) 8–12.